Title	Eccentricity effect of micropatterned surface on contact angle
Author(s)	Kashaninejad, Navid; Chan, Weng Kong; Nguyen, Nam-Trung
Citation	Kashaninejad, N., Chan, W. K., & Nguyen, N. T. (2012). Eccentricity effect of micropatterned surface on contact angle. Langmuir, 28(10), 4793-4799.
Date	2012
URL	http://hdl.handle.net/10220/7825
Rights	© 2012 American Chemical Society. This is the author created version of a work that has been peer reviewed and accepted for publication in Langmuir, published by American Chemical Society. It incorporates referee's comments but changes resulting from the publishing process, such as copyediting, structural formatting, may not be reflected in this document. The published version is available at: http://dx.doi.org/10.1021/la300416x.

Eccentricity Effect of Micropatterned Surface on Contact Angle

Navid Kashaninejad, Weng Kong Chan, and Nam-Trung Nguyen*

School of Mechanical and Aerospace Engineering, Nanyang Technological University, Singapore 639798

***** *Corresponding author. E-mail: mntnguyen@ntu.edu.sg*

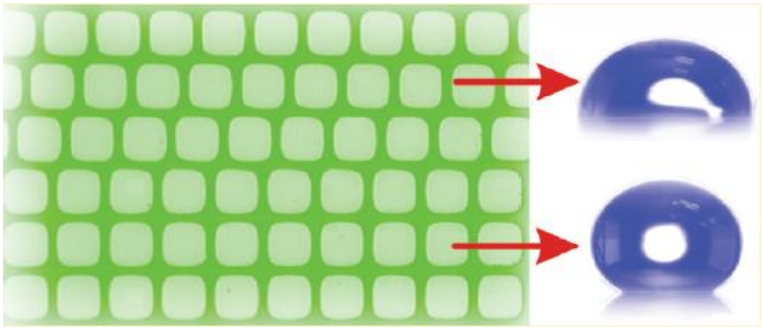

ABSTRACT: This article experimentally shows that the wetting property of a micropatterned surface is a function of the center-to-center offset distance between successive pillars in a column, referred to here as eccentricity. Studies were conducted on square micropatterns which were fabricated on a silicon wafer with pillar eccentricity ranging from 0 to 6 μm for two different pillar diameters and spacing. Measurement results of the static as well as the dynamic contact angles on these surfaces revealed that the contact angle decreases with increasing eccentricity and increasing relative spacing between the pillars. Furthermore, quantification of the contact angle hysteresis (CAH) shows that, for the case of lower pillar spacing, CAH could increase up to 41%, whereas for the case of higher pillar spacing, this increment was up to 35%, both corresponding to the maximum eccentricity of 6 μm. In general, the maximum obtainable hydrophobicity corresponds to micropillars with zero eccentricity. As the pillar relative spacing decreases, the effect of eccentricity on hydrophobicity becomes more pronounced. The dependence of the wettability conditions of the micropatterned surface on the pillar

eccentricity is attributed to the contact line deformation resulting from the changed orientation of the pillars. This finding provides additional insights in design and fabrication of efficient micropatterned surfaces with controlled wetting properties.

1. INTRODUCTION

Evaluating the contact angle behavior of a solid surface is of great importance for many practical applications such as self-cleaning coatings, surface tension driven flow in micro-electromechanical- systems (MEMS), and drag reduction of film liquid flow in micro/nanochannels. It is well-known that micro/nano arrays of pillars on a surface can greatly affect the contact angle. The wetting properties of artificially roughened surface referred to here as micropatterned surface have been evaluated extensively in the literature.[1−6] Two extreme situations may occur on these micropatterned surfaces. First, the droplet may penetrate into the gap between the pillars known as noncomposite state; and second, the droplet may stay on top of the pillars enclosing air pockets termed as composite state. The noncomposite and the composite states were evaluated by Wenzel[1] and Cassie−Baxter,[2] respectively. The contact angle was determined as a function of intrinsic contact angle as well as roughness geometry with parameters such as roughness factor and wetted area of solid fraction. Part a of Figure 1 illustrates the side view of a typical micropatterned surface with geometrical parameters such as width (top L, bottom l), base angles (top α, bottom β), height h, and spacing D. In the same figure, ζ depicts the height of an air gap underneath the liquid drop, which is 0 for noncomposite state and h for composite state.

Park et al.[7] reported that depending on the relative values of pillar spacing and heights, observed wetting states could be considered as mixed wetting state, that is, $0 < \zeta/h < 1$, . The liquid−air meniscus could either be convex or concave for hydrophobic or hydrophilic pillars, respectively. Chen et al.[8] introduced a dimensionless number as a function of pillar height and size, and experimentally showed that a large apparent contact angle is achievable with this number larger than 4 and a small solid fraction. Oner and McCarthy[9] investigated the dynamic hydrophobicity of extensive micropatterned surfaces and reported that as long as the length scale of the square micropillars, with the

equal spacing and size less than 32 μm, composite state with large contact angle and small contact angle hysteresis could be obtained regardless of the pillar height. They also observed that changing the pillar shape would affect the dynamic contact angle, which is not predictable by Cassie−Baxter theory. Extrand[10] introduced the two criteria ensuring the composite state, namely, the contact line density and the asperity height. To identify the role of the factors determining the wettability condition of the micropatterned surface, Li and Amirfazli[11,12] performed a comprehensive theoretical work based on free energy and free energy barrier of a metastable energy state, which was the simplified version of the 3D approach previously proposed by Johnson and Detree.[13] The obtained analytical formula clearly explained how geometrical parameters of a pillar affect the wetting conditions.[12] Li et al.[14] extended the previous analysis for the trapezoidal micropatterns and concluded that pillar base angle α in part a of Figure 1 was also important in determining the transition from the composite state to the noncomposite one.

The applicability of Cassie−Baxter and Wenzel theories were supported but in some cases questioned by various researchers over the years.[15−29] From the thermodynamic point of view, the contact angle on any surface can be determined by minimization of the Gibbs free energy, *G*, whose change can be formulated as follows:[30]

$$\delta G = \gamma_{SL}\delta A_{SL} + \gamma_{SV}\delta A_{SV} + \gamma_{LV}\delta A_{LV} + \Delta P \mathrm{d}V - k\mathrm{d}l \quad (1)$$

where γ denotes the interfacial surface energy and subscripts S, L, and V correspond to solid, liquid, and vapor phases, respectively. The change in volume of the drop dV, as a result of the change in the Laplace pressure (ΔP), is negligible for incompressible substances. The line tension or energy per unit length *k* is associated with a length increment in the three-phase contact line d*l*. The effect of changing the three-phase contact line has been neglected in derivations of the both Cassie−Baxter and Wenzel formula and is the main reason of the long dispute in the literature regarding these theories. For example, Chen et al.[31] demonstrated that surfaces with the same solid−liquid

area fractions can have different contact angles, which proved the importance of the three-phase contact line. Similarly, Extrand[32] showed that interactions at the contact line and not the contact area controls wetting of heterogeneous surfaces. Gao and McCarthy[20] also showed a large deviation between experimentally measured contact angles and those predicted by the Cassie−Baxter equation. Anantharaju et al.[33] experimentally compared two situations differing only in the microstructure of the roughness. The results showed that the contact angle on surfaces with microholes was independent of the void fraction due to the continuity of the contact line.

Therefore, it seems that apart from those geometrical parameters predicted by classical wetting theories and those addressed in the previous works (part a of Figure 1), other factors influencing the topology of the three-phase contact line should also be taken into account in evaluating wetting behavior. One of these factors is the orientation of the pillars, in particular the center-to-center offset distance between successive pillars in a column. This distance is called in our present work as the eccentricity ε. This parameter is represented in part b of Figure 1. This parameter can also be regarded as how much the pillars of a micropatterned surface deviates from being symmetric. Therefore, by changing this parameter, the surface is no longer isentropic and becomes directional dependence. This directional dependency known as anisotropic wetting is not only a peculiar phenomenon but also common in some natural surfaces such as rice leaves,[34] which have the ability to directionally control the movement of water droplets.[35] Anisotropic wetting of the 1D strips of hydrophobic and hydrophilic regions as well as 2D microgroove have already been evaluated in the literature[28,36] and the effect of changing the viewing direction along and across the groove on the contact angle was reported and it was found that Cassie−Baxter equation was only valid when the contact line moved along the strip.[28] As Cassie−Baxter emphasized in their original work,[2] anisotropic wetting was completely different along the perpendicular direction. However, the effect of anisotropic wetting on discrete pillars was not evaluated in the literature, and thus evaluating the wetting conditions by changing both pillar eccentricity as well as viewing directions would make the analysis much more complex. Therefore, in the

present article, all contact angles were measured along a fixed direction, the y direction shown in part a of Figure 2, whereas the pillar eccentricity was changed systematically.

To the best knowledge of the authors, the eccentricity effects of the micropatterned surface on contact angle values have not been investigated before and will be the main focus of our present work. Studies were conducted on square micropatterns, which are fabricated on silicon wafers with pillar eccentricity ranging from 0 to 6 μm for two different pillar spacing values. By measuring of the static as well as the dynamic contact angles on these surfaces, the eccentricity effects on dynamic hydrophobicity will also be investigated.

2. EXPERIMENTAL METHOD

2.1. Design of Micropillars. To evaluate the effect of pillar orientation on wetting conditions, pillars with identical square shape (Figure 2), height (H = 8 μm), width (L), and spacing (D) but different eccentricity (ε) were designed and fabricated on a silicon substrate. As inferred from eq 1, the value of the contact angle can also be a function of k, which can be defined as the force (energy) required to pin the unit length (area) of the drop to the surface. Thus, this term depends on the fraction of the solid wetted by the drop, that is, the smaller the fraction, the lower is the pinning of the contact line, or the lower is the value of k. Consequently, it is worth comparing the wetting behavior at different pillar density, determined by the ratio L/D. In a different set of experiments, pillars with the same variation of eccentricity (0−6 μm) but lower pillar density were investigated. The detailed geometrical values of these pillar structures are listed in Table 1. It is also more meaningful to consider the dimensionless values of pillar parameters. Throughout this paper the superscript (*) indicates the relative pillar size with respect to its size, that is, $D^* = D/L$ and $\varepsilon^* = \varepsilon/L$.

2.2. Fabrication Processes. The pillar geometries were designed and patterned on a glass mask. Since positive photoresist (AZ4620) was used during photolithography, the pillars on the mask appear opaque, so that the patterns of the pillars would remain on the wafer.

Silicon wafers were cleaned with piranha following RCA (Radio Corporation of America) procedure to achieve maximum process reliability. After the cleaning process, the wafer was dried by blowing with nitrogen gas and then baked at 100 ℃ for 1 min on a hot plate. Prebake was required to improve the surface adhesion of the silicon wafer before the coating process. The wafer was baked at 100 ℃ for 90 s. Two-step coating of the photoresist AZ4620 was applied to achieve uniform resist on the silicon wafer. The first step slowly spreads the resist on the whole wafer surface. The second step distributes the resist uniformly. The coated wafer was then soft baked at 100 ℃ for 90 s on a hot plate to remove excess solvent and to improve the adhesion of photo resist on the wafer. Next, the wafer was exposed to UV light for about 170 s at an intensity of 8.3 mW/cm^2.

As the photoresist used was a positive type, exposed region of the resist was removed, leaving the unexposed photoresist on the wafer. The developer was diluted with deionized (DI) water with a volume ratio of 1:4 to gain more control over the development process of the photoresist. The wafer was examined under a microscope to ensure that there were no residues of photoresist on the patterns of the wafer as it would affect the etching process. If there were still some residues, the wafer was immersed again in the developer until the resist was completely removed. The silicon wafer with the patterns was subsequently rinsed in DI water and slowly dried by nitrogen gas.

Before etching the actual wafer, the etch rate was determined by measuring the depth of the etched wafer and the etching time. With an etch rate of about 3 μm per minute, the time required for etching 8 μm depth is 160 s. A representative image of such fabricated micropillars along with the related parameters is shown in Figure 2.

2.3. Contact Angle Measurement. Prior to measuring the contact angle, the Si wafers were thoroughly treated and cleaned as follows. The wafers were immerged in acetone and placed in an ultrasound cleaner for 5 min. Next, isopropanol was used to remove the remaining acetone from the samples. Finally, the wafer were thoroughly washed with DI water and dried by nitrogen gas.

The commercial tensiometer FTA200 (First Ten Ångstroms, Portsmouth, VA, USA) was used to measure the contact angles and wettability conditions of the micropatterned surfaces. As mentioned before, due to the anisotropic structure of the pillars, all the contact angles were measured along the same viewing direction along *y* axis as shown in part a of Figure 2. To ensure the spherical geometry of the drop where surface tension is dominant rather than weight, the maximum volume of the droplet was selected to be 30 μL. The Bond number B_o indicates the relative importance of the weight to surface tension force. For $\theta = 90°$ and the maximum drop volume of $V = 3e^{-8}\text{m}^3$, the Bond number is $B_o = (\rho g r^2)/\gamma = 0.8$, where $\gamma = 72$ mN/m is the surface tension of water at 25 °. The radius of the drop can be estimated from the volume of the drop as $r = [3/\pi(\sin^3\theta\forall)/(2 - 3\cos\theta - 3\cos^3\theta)]^{1/3}$. Therefore, the effect of gravity on the droplet can be neglected. To measure the static contact angle of the droplet, a small volume of DI water ($V = 10$ μL) was placed carefully on the surface of each sample. When the droplet has stabilized, its image was captured and analyzed using FTA200. The corresponding contact angle was then evaluated. The advancing and receding contact angles were also measured using the so-called imbedded needle technique using the same instrument. To measure the advancing contact angle, the droplet volume was increased very slowly at a rate of 0.5 μL/s from its initial volume of 5 μL to the maximum volume of 30 μL. Whereas the contact line of the droplet remains fixed, the contact angle increases with increasing volume of the droplet. When the droplet reaches a specific volume, further increment of the droplet volume causes the contact line to move. At this moment, pumping was stopped and the contact angle just before the expansion of the contact line was recorded as the advancing contact angle. The reverse process was done to measure the receding contact angle.

The pixel error in FTA200 is reported to be around 0.5 degrees. All of the measurements were conducted at least five times at different locations on the sample. The reported contact angles are the mean values. The standard deviations were calculated from the data set. The average values of the measured static and dynamic contact angles (i.e., advancing and receding contact angles) and the statistical errors are listed in Table 2.

Typical values of the measured contact angles are illustrated in Figure 3. A bare, smooth silicon substrate has an advancing contact angle of 65°, as seen in part a of Figure 3. By patterning the pillars on the surface, the contact angle increases, as seen in part b of Figure 3. In the case depicted in part c of Figure 3, the effect of eccentricity can be seen by comparing with part b of Figure 3. In both cases, pillar relative spacing is 0.2 whereas eccentricity changes from the maximum to the minimum value. The results show that the contact angle of micropatterned surfaces with the same pillar geometry increases from 95° to 119° just by decreasing the eccentricity from 6 to 0 μm. Part d of Figure 3 represents the sample with the pillars of the same height and eccentricity as those depicted in part c of Figure 3 but with a larger relative spacing. In this case, the apparent contact angle increases significantly. This observation is consistent with the Cassie−Baxter theory, which predicts that surfaces with lower solid−liquid area fraction have higher contact angle values.

3. RESULTS AND DISCUSSIONS

The measured contact angles for the different micropillar patterns listed in Table 1 are presented graphically in Figures 4 to 6. In Figure 4, the static contact angles on the micropatterned silicon surfaces are plotted versus the normalized eccentricity, $\varepsilon^* = \varepsilon/L$ for two different normalized spacing $D^* = D/L$. First, the results show that patterning the surface of the silicon substrate with micro pillars increases the contact angle. In the experiments, the droplet was gently placed on the surface, that is at approximately zero velocity. However, it was also observed that a high impact velocity of the droplet can impose higher pressure causing the droplet to penetrate into the pillar spacing and consequently decreases the contact angle. Therefore, measured values of the contact angle can be considered in a state where the water droplet has the minimum contact with the surface, that is the composite state. Second, increasing the relative spacing between the pillars from 0.2 to 0.4 by decreasing the pillars' size and increasing the spacing between them significantly increases the contact angle by almost 20°. This result confirms that the liquid droplet on top of the pillar is in the composite state.

The most important result of this experiment, also the main objective of our study, is the variation of contact angle by changing the eccentricity of the micropillars. Figure 4 shows that the contact angle is a linear function of eccentricity and the gradient is inversely proportional to the pillar relative spacing D^*. As observed, for the case of higher pillar density (lower relative air gap $D^* = 0.2$, the apparent contact angle decreases from 119 ° to 103 ° as the eccentricity of the micropillars increases from 0 to 6 μm). This indicates that more than 13% reduction in contact angle is caused by the increment of eccentricity. The higher the pillar relative spacing or the lower the pillar density, the less is the dependency of the static contact angle on the pillar eccentricity.

Dynamic contact angles of the droplet on the samples are shown in Figures 5 and 6 for the respective pillar spacing. The trend of change in advancing and receding contact angles is qualitatively the same as the static contact angle discussed above.

Figures 5 and 6 also depict the contact angle hysteresis (CAH), which is the difference between advancing contact angle $\theta_{advancing}$ and receding contact angle $\theta_{receding}$. CAH is an important parameter characterizing the hydrophobicity of the samples. A high value of CAH corresponds to the case where the three-phase contact line is pinned to the pillars. Therefore, CAH can be related to the line tension k in eq 1. In other words, the difference between the advancing and the receding contact angle is due to the effect of three-phase contact line. As shown in Figures 5 and 6, increasing the relative spacing between the pillars decreases the CAH and increases hydrophobicity. On surfaces with lower spacing ($D^* = 0.2$), increasing the eccentricity from 0 to 6 μm also increases CAH, as seen in Figure 5. This trend implies that hydrophobicity of the droplet is inversely proportional to eccentricity. The trend of CAH in Figure 6 leads to the same conclusion. For better understanding the trend of increasing CAH $\Delta\theta$ as a function of pillar eccentricity, the following nondimensional variable is defined:

$$\Delta\theta^* = \frac{\Delta\theta(\varepsilon) - \Delta\theta(0)}{\Delta\theta(0)} \times 100\% \qquad (2)$$

where $\Delta\theta(\varepsilon)$ is the CAH at different values of eccentricity, $\Delta\theta(0)$ is the CAH at zero eccentricity, corresponding to minimum CAH.

For the investigated samples, $\Delta\theta^*$ is plotted against the normalized eccentricity for both cases of low and high pillar spacing, Figure 7. Figure 7 reveals that at a maximum eccentricity of 6 μm CAH can increase up to 41% for lower pillar spacing and 35% for higher pillar spacing. For both cases of higher and lower pillar spacing, maximum obtainable hydrophobicity corresponds to the pillar patterns with zero eccentricity. As the pillar relative spacing decreases, the effect of increasing the eccentricity becomes much more pronounced.

Dependency of contact angles as well as CAH on pillar eccentricity cannot be explained by the original form of Cassie−Baxter equation since the effect of three-phase contact line was neglected as mentioned in the introduction. Drelich et al.[37] derived the modified version of this equation by taking into account the effect of contact line tension k for a surface consisting of n heterogeneous structures, as follows:

$$\cos\theta_C^M = \sum_{i=1}^{n} \varphi_{si}\cos\theta_i - \frac{1}{\gamma_{LV}} \sum_{i=1}^{n} \varphi_{si} k_i \frac{1}{\mathcal{R}_i} \qquad (3)$$

In eq 3, θ_C^M is the modified Cassie contact angle, φ_S is the wetted area of the solid fraction, γ_{LV} is interfacial tension of liquid and vapor, and $\mathcal{R}$ is the radius of curvature of the three-phase contact line. The first term on the right-hand side is the same originally derived by Cassie.[38] The second term is the additional term due to the existence of the contact line tension. According to the above equation, the effect of this additional term becomes important in two situations. First, the contact line is pinned to the pillars where the role of line tension k is significant. Second, the radius of curvature $\mathcal{R}$ is small. Eq 3 indicates that, for the radii of deformation on the order of several micrometers, the effect of contact line should be taken into account.[39] Also, different contact line corrugations may lead to different values of contact angle despite the constant Cassie term.[40] The possible presentation of the three-phase contact line is illustrated schematically in parts a

and b of Figure 8 for a micropatterned surface with zero and nonzero eccentricity, respectively. This hypothesis agrees with the observation made in our experiment. Changing the pillar eccentricity while keeping the solid area fraction constant may lead to a change in contact line radius of curvature and consequently a change in the apparent contact angle.

Furthermore, we found that the influence of contact angle as well as CAH variations with eccentricity is more pronounced for pillars with a smaller relative spacing D^* which also can be derived from eqs 1 and 3. It was well-known and also shown in our current work that increasing pillar spacing makes the wetting state becomes closer to the composite state, for example, $\zeta \rightarrow h$ as shown in part a of Figure 1.The three-phase contact line depins from the pillar because of the small contact line tension k. Consequently CAH is smaller and the surface becomes more hydrophobic. Comparing Figures 5 and 6, our experimental results confirm the increase of CAH by increasing the pillars relative spacing. This also implies that the line tension is smaller for the case of higher pillar spacing. At the smaller values of line tension corresponding to the higher pillar spacing, the effect of deformation of the three-phase contact line (dl and $1/\mathcal{R}_i$ in eqs 1 and 3) on the contact angle as well as CAH becomes insignificant. The reverse is true for the case of lower relative pillar spacing. This fact is in complete agreement with the current experimental results.

4. CONCLUSIONS

This article investigated the effect of an additional pillar geometrical parameter, termed as eccentricity, on the dynamic wettability conditions of micropatterned surfaces. Micropillar arrays with sizes ranging from 6 and 7 μm, a constant height of 8 μm, spacing of 1.5 and 2.5 μm, and variable eccentricities from 0 to 6 μm were fabricated on silicon wafers using photolithography and etching. Static and dynamic contact angles were measured by placing a small volume (5 μL $\leq V \leq$ 30 μL) of DI water droplet gently onto the fabricated surfaces. The high contact angle and the metastable wetting condition as observed in the experiments confirm that the water droplet stays on top of the pillar. At zero eccentricity, by increasing the relative spacing between the pillars, an increase in

static contact angle of more than 20 ° (from 119 ° to 141 °) and a decrease of the CAH (from 17 ° to 24 °) was observed. The measured static and dynamic contact angles were found to be a descending linear function of pillar eccentricity. The gradient is inversely proportional to the pillar relative spacing. At a maximum eccentricity of 6 μm CAH can increase up to 41% for the lower pillar spacing, and 35% for the higher pillar spacing. The maximum obtainable hydrophobicity corresponds to micropillars with zero eccentricity. As the pillar relative spacing decreases, the effect of increasing the eccentricity in decreasing the hydrophobicity becomes much more pronounced. These findings can be explained by taking into account the additional term of three-phase contact line tension using the modified Cassie eq 3. Changing the pillar eccentricity causes the three-phase contact line to deform at different radii of curvature, which affect the contact angle. The effect of varying pillar eccentricity on contact angle is more pronounced with low spacing micropillars. This observation agrees with the modified Cassie equation where at lower pillar spacing, three-phase contact line tends to pin to the pillars and the order of line tension becomes more significant. In that case, the additional term due to the effect of three-phase contact line in eq 3 becomes more important. Finally, it can be concluded that the eccentricity of the pillar arrays beside other pillar geometrical parameters, should also be taken into account to design micropatterned surface with controlled wettability and micropillars with zero eccentricity being more hydrophobic.

REFERENCES

(1) Wenzel, R. N. *Resistance of Solid Surfaces to Wetting by Water. Ind. Eng. Chem.* **1936**, *28* (8), 988−994.

(2) Cassie, A. B. D.; Baxter, S. *Wettability of porous surfaces. Trans. Faraday Soc.* **1944**, *40*, 546−551.

(3) Dettre Robert, H. Johnson Rulon, E., *Contact Angle Hysteresis*, In *Contact Angle, Wettability, and Adhesion*, American Chemical Society: Washington D.C., 1964; p 136−144.

(4) He, B.; Patankar, N. A.; Lee, J. *Multiple Equilibrium Droplet Shapes and Design Criterion for Rough Hydrophobic Surfaces. Langmuir* **2003**, *19* (12), 4999−5003.

(5) Patankar, N. A. *On the modeling of hydrophobic contact angles on rough surfaces. Langmuir* **2003**, *19* (4), 1249−1253.

(6) Nakae, H.; Yoshida, M.; Yokota, M. *Effects of roughness pitch of surfaces on their wettability. J. Mater. Sci*. **2005**, *40* (9), 2287−2293.

(7) Park, C. I.; et al. *Wetting transition and optimal design for microstructured surfaces with hydrophobic and hydrophilic materials. Journal of colloid and interface science* **2009**, *336* (1), 298−303.

(8) Chen, L. Y. K. Lee. *New dimensionless number for superhydrophobicity study of micron/submicron patterned surfaces. IEEE.*

(9) Öner, D.; McCarthy, T. J. *Ultrahydrophobic surfaces. Ef fects of topography length scales on wettability. Langmuir* **2000**, *16* (20), 7777−7782.

(10) Extrand, C. *Criteria for ultralyophobic surfaces. Langmuir* **2004**, *20* (12), 5013−5018.

(11) Li, W.; Amirfazli, A. A *thermodynamic approach for determining the contact angle hysteresis for superhydrophobic surfaces. J. Colloid Interface Sci*. **2005**, *292* (1), 195−201.

(12) Li, W.; Amirfazli, A. *Microtextured superhydrophobic surfaces: A thermodynamic analysis. Adv. Colloid Interface Sci*. **2007**, *132* (2), 51−68.

(13) Johnson, R.; Dettre, R. H. *Contact angle hysteresis. Contact Angle, Wettability, and Adhesion. Advances in Chemistry Series* **1964**, *43*, 112−135.

(14) Li, W.; Cui, X.; Fang, G. *Optimal Geometrical Design for Superhydrophobic Surfaces: Ef fects of a Trapezoid Microtexture. Langmuir* **2010**, *26* (5), 3194−3202.

(15) Swain, P. S.; Lipowsky, R. *Contact angles on heterogeneous surfaces: a new look at Cassie's and Wenzel's laws. Langmuir* **1998**, *14* (23), 6772−6780.

(16) Oner, D.; McCarthy, J. *Ultrahydrophobic Surfaces. Ef fects of Topography Length Scales on Wettability. Langmuir* **2000**, *16*, 7777−7782.

(17) Marmur, A. *Wetting on hydrophobic rough surfaces: to beheterogeneous or not to be? Langmuir* **2003**, *19* (20), 8343−8348.

(18) Jopp, J.; Grüll, H.; Yerushalmi-Rozen, R. *Wetting behavior of water droplets on hydrophobic microtextures of comparable size. Langmuir* **2004**, 20 (23), 10015−10019.

(19) Callies, M.; et al. *Microfabricated textured surfaces for superhydrophobicity investigations. Microelectron. Eng*. **2005**, *78*, 100−105.

(20) Gao, L.; McCarthy, T. J. *How Wenzel and Cassie were wrong. Langmuir* **2007**, *23* (7), 3762−3765.

(21) McHale, G. *Cassie and Wenzel: were they really so wrong? Langmuir* **2007**, *23* (15), 8200−8205.

(22) Nosonovsky, M. *On the range of applicability of the Wenzel and Cassie equations. Langmuir* **2007**, *23* (19), 9919−9920.

(23) Panchagnula, M. V.; Vedantam, S. *Comment on how Wenzel and Cassie were wrong by Gao and McCarthy. Langmuir* **2007**, *23* (26), 13242−13242.

(24) Gao, L.; McCarthy, T. J. *Reply to "comment on how Wenzel and Cassie were wrong by Gao and McCarthy". Langmuir* **2007**, *23* (26), 13243−13243.

(25) Bormashenko, E. *Why does the Cassie-Baxter equation apply? Colloids Surf., A* **2008**, *324* (1−3), 47−50.

(26) Marmur, A.; Bittoun, E. *When Wenzel and Cassie are right: Reconciling local and global considerations. Langmuir* **2009**, *25* (3), 1277−1281.

(27) Gao, L.; McCarthy, T. J. *An attempt to correct the faulty intuition perpetuated by the Wenzel and Cassie "laws". Langmuir* **2009**, *25* (13), 7249−7255.

(28) Choi, W.; et al. *A modif ied Cassie-Baxter relationship to explain contact angle hysteresis and anisotropy on non-wetting textured surfaces. J. Colloid Interface Sci*. **2009**, *339* (1), 208−216.

(29) Kwon, Y.; et al. *Is the Cassie− Baxter Formula Relevant? Langmuir* **2010**.

(30) Tadmor, R. *Line energy and the relation between advancing, receding, and young contact angles. Langmuir* **2004**, *20* (18), 7659−7664.

(31) Chen, W.; et al. *Ultrahydrophobic and ultralyophobic surfaces: some comments and examples. Langmuir* **1999**, *15* (10), 3395−3399.

(32) Extrand, C. *Contact angles and hysteresis on surfaces with chemically heterogeneous islands. Langmuir* **2003**, *19* (9), 3793−3796.

(33) Anantharaju, N.; et al. *Effect of three-phase contact line topology on dynamic contact angles on heterogeneous surfaces. Langmuir* **2007**, *23*(23), 11673−11676.

(34) Feng, L.; et al. *Super-hydrophobic surfaces: From natural to artificial. Advanced materials* **2002**, *14* (24), 1857−1860.

(35) Wu, D.; et al. *Three-level biomimetic rice-leaf surfaces with controllable anisotropic sliding. Adv. Funct. Mater*. **2011**.

(36) Xia, D.; et al. *Tailoring anisotropic wetting properties on submicrometer-scale periodic grooved surfaces. Langmuir* **2010**, *26* (4), 2700−2706.

(37) Drelich, J.; Miller, J. D. *Modification of the Cassie equation. Langmuir* **1993**, *9* (2), 619−621.

(38) Cassie, A. *Contact angles. Discuss. Faraday Soc*. **1948**, *3*, 11−16.

(39) Drelich, J.; Miller, J. D. *The line/pseudo-line tension in three-phase systems. Particulate science and technology* **1992**, *10*, 1−1.

(40) Ruiz-Cabello, F. J. M.; et al. *Modeling the corrugation of the threephase contact line perpendicular to a chemically striped substrate. Langmuir* **2009**, *25* (14), 8357−8361.

List of Tables

List of Figures

Fig. 8 Possible illustration of the three-phase contact line: (a) pillars with zero eccentricity; (b) pillars with nonzero eccentricity.

L (μm)	D (μm)	ε (μm)	$D^* = D/L$
7	1.5	0, 2, 4, 6	0.2
6	2.5	0, 2, 4, 6	0.4

Table 1

D^*	ε^*	θ_{static} (°)	$\theta_{advancing}$ (°)	$\theta_{receding}$ (°)
0.2	0	119 ± 4	125 ± 4	101 ± 5
	0.28	114 ± 4	120 ± 4	95 ± 6
	0.57	112 ± 5	118 ± 4	87 ± 6
	0.85	103 ± 5	111 ± 5	77 ± 6
0.4	0	141 ± 2	145 ± 3	127 ± 5
	0.33	140 ± 4	144 ± 3	121 ± 6
	0.66	134 ± 4	139 ± 4	118 ± 5
	1	141 ± 2	143 ± 4	120 ± 6

Table 2

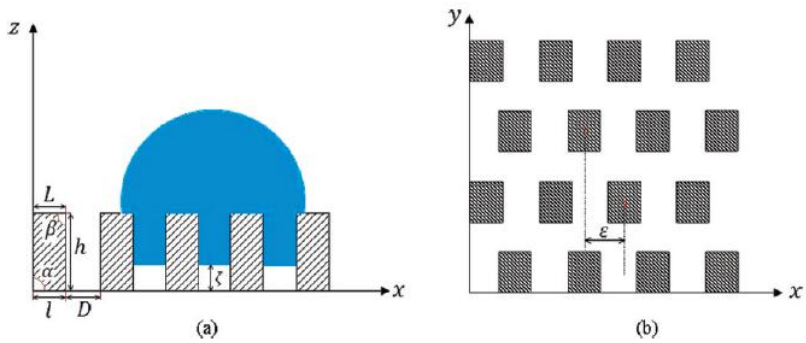

Fig. 1

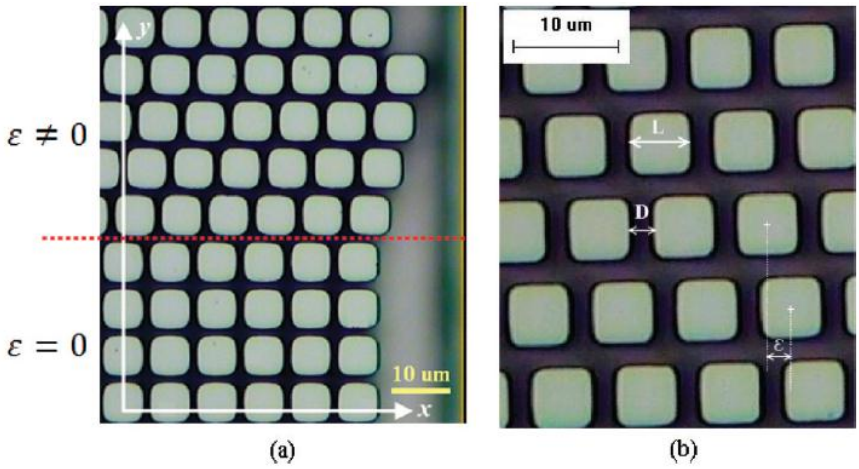

Fig. 2

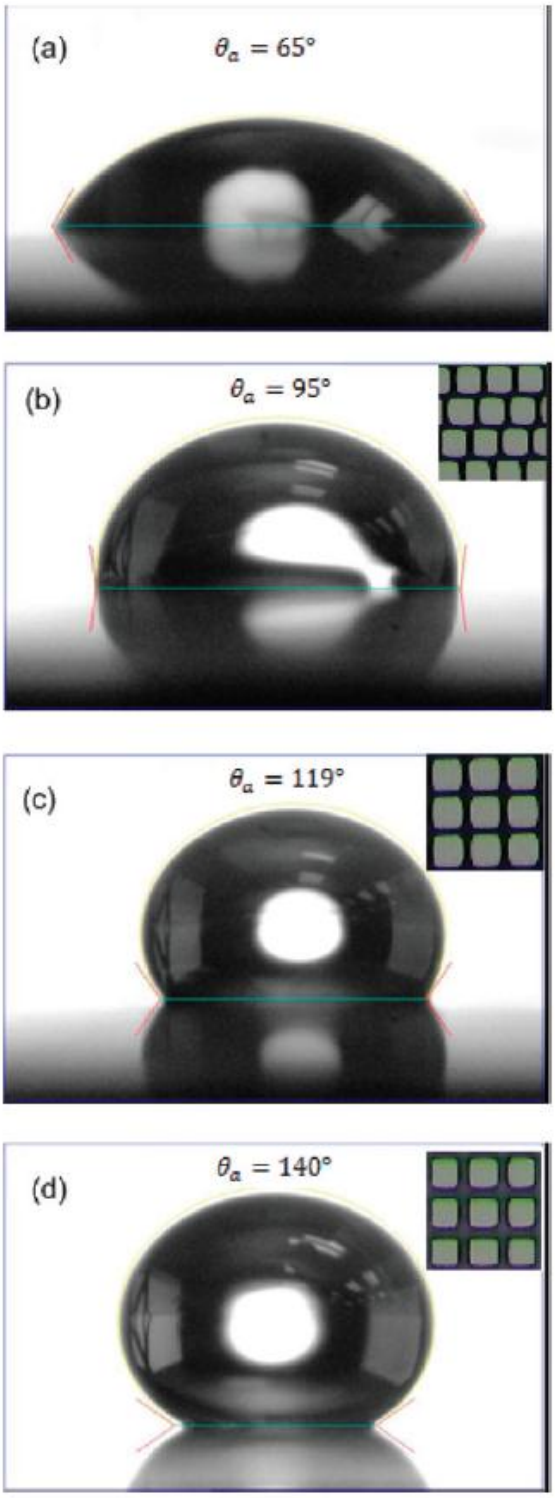

Fig. 3

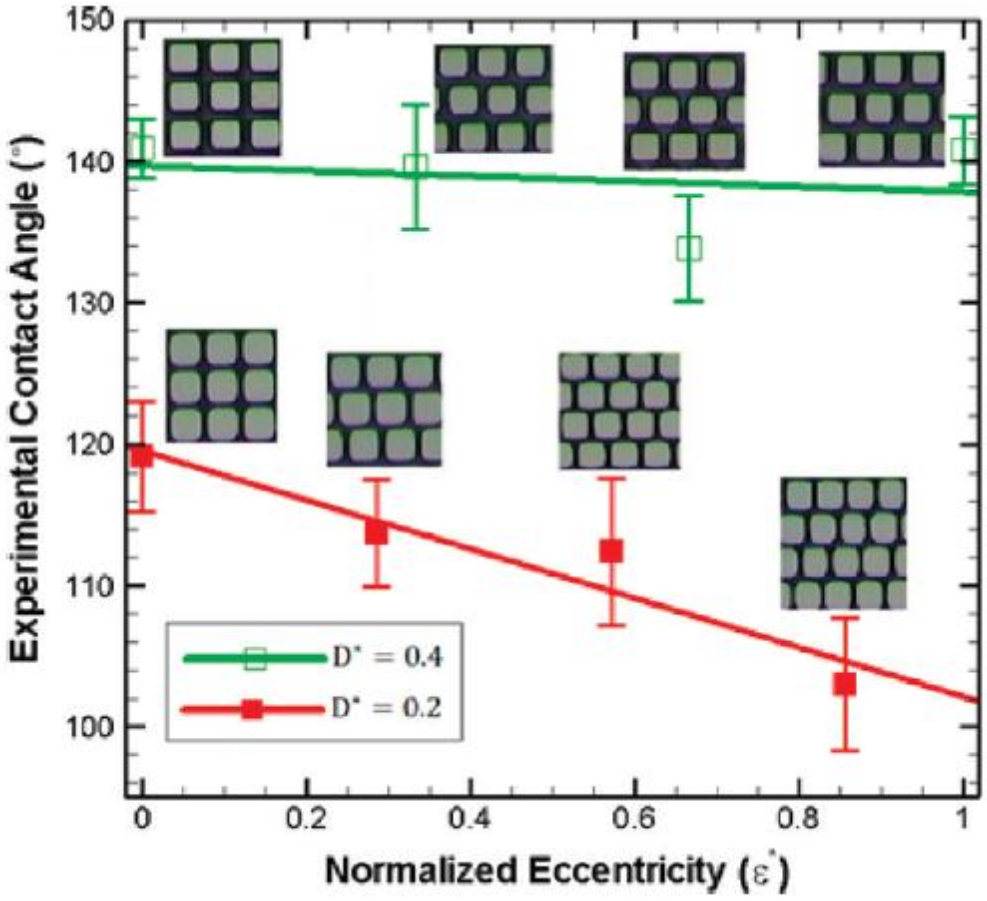
Experimental Contact Angle (°)
150
140
130
120
110
100
0
0.2
0.4
0.6
0.8
1
Normalized Eccentricity (ε*)
D* = 0.4
D* = 0.2

Fig. 4

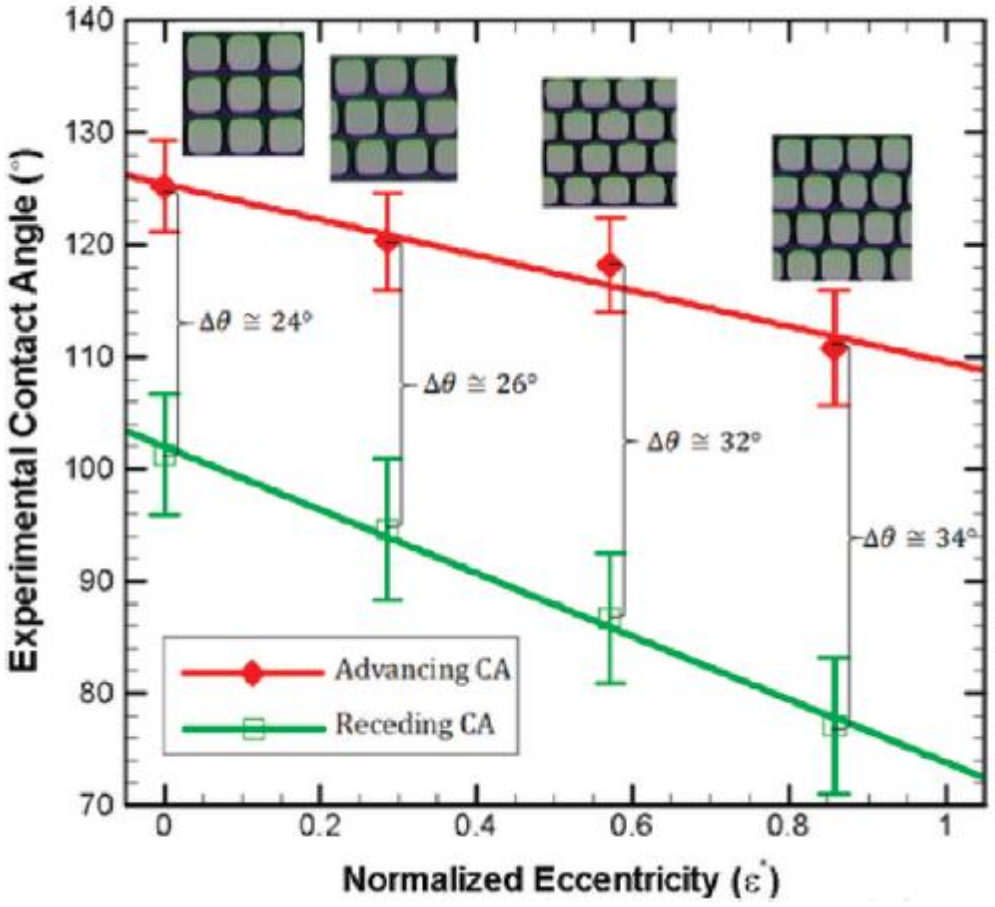
Experimental Contact Angle (°)
Normalized Eccentricity (ε*)
Advancing CA
Receding CA
Δθ ≅ 24°
Δθ ≅ 26°
Δθ ≅ 32°
Δθ ≅ 34°
140
130
120
110
100
90
80
70
0
0.2
0.4
0.6
0.8
1

Fig. 5

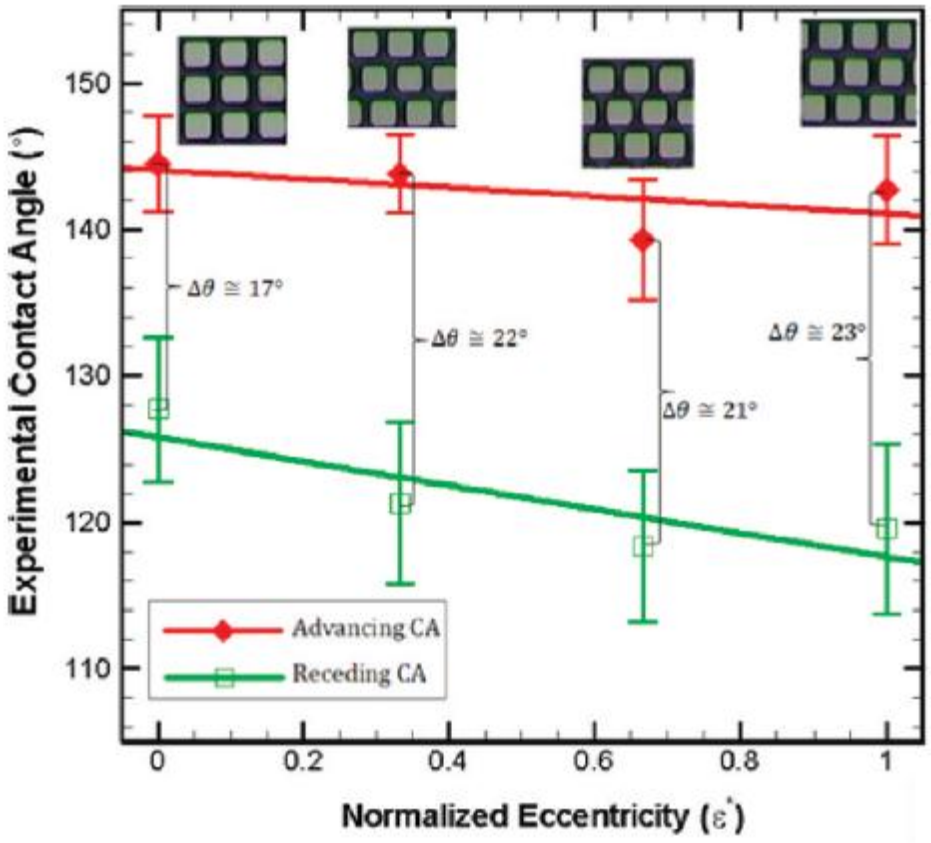
Experimental Contact Angle (°)
150
140
130
120
110
0
0.2
0.4
0.6
0.8
1
Normalized Eccentricity (ε*)
Δθ ≅ 17°
Δθ ≅ 22°
Δθ ≅ 21°
Δθ ≅ 23°
Advancing CA
Receding CA

Fig. 6

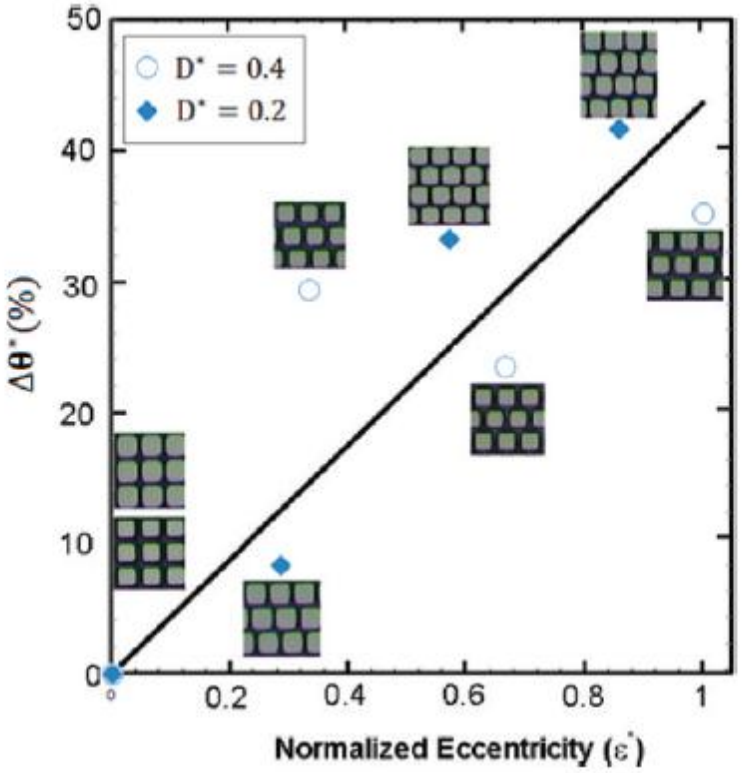
D* = 0.4
D* = 0.2
50
40
30
20
10
0
0
0.2
0.4
0.6
0.8
1
Δθ* (%)
Normalized Eccentricity (ε*)

Fig. 7

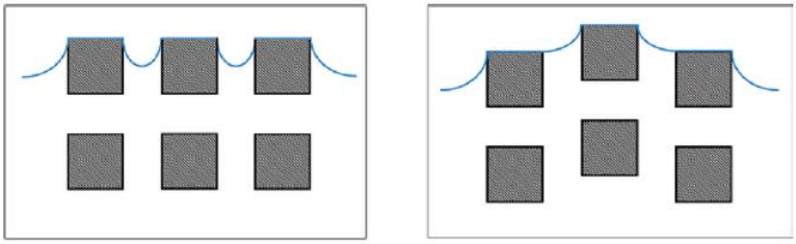

Fig. 8